Supplementary Information for:

Copper(I) Bis(diimine) Sensitized Titania Nanotube Array Photoelectrodes for Photoelectrochemical Water Oxidation

Joseph D. Chiong[1,2], Zujhar Singh[1], Joseph F. Ricardo-Noordberg[1], Nhat Truong Nguyen[2]*, Marek B. Majewski[1]*

1. Department of Chemistry and Biochemistry and Centre for NanoScience Research Concordia University 7141 Sherbrooke Street West, Montreal, Quebec, Canada, H4B 1R6

2. Department of Chemical and Materials Engineering 1455 De Maisonneuve Boulevard West, Montreal, Quebec, Canada, H3G 1M8

E-mail: marek.majewski@concordia.ca; truong.nguyen@concordia.ca

Contents

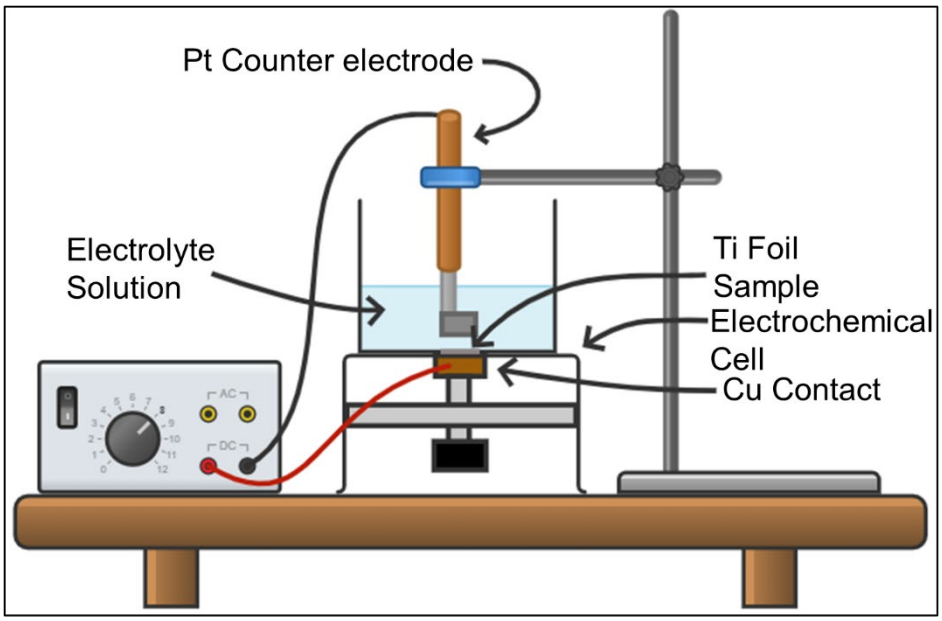

Scheme S1. Self-organized electrochemical anodization (SOA) setup using a custom-made electrochemical cell.

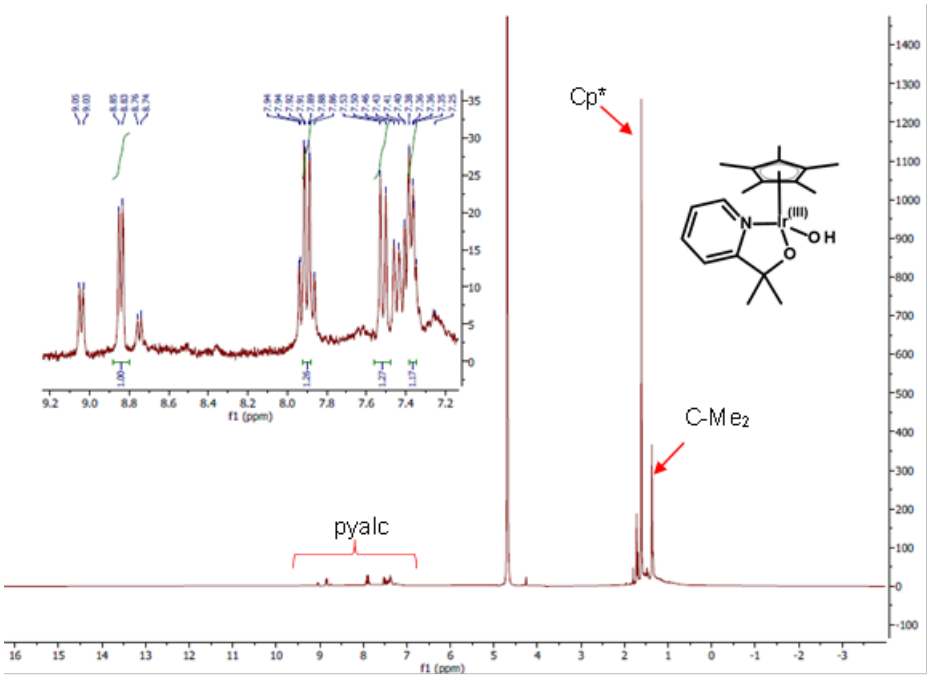

Figure S1. ^{1}H NMR spectrum of [Cp*Ir(pyalc)OH] in $CDCl_3$ recorded on a 300 MHz Bruker spectrometer

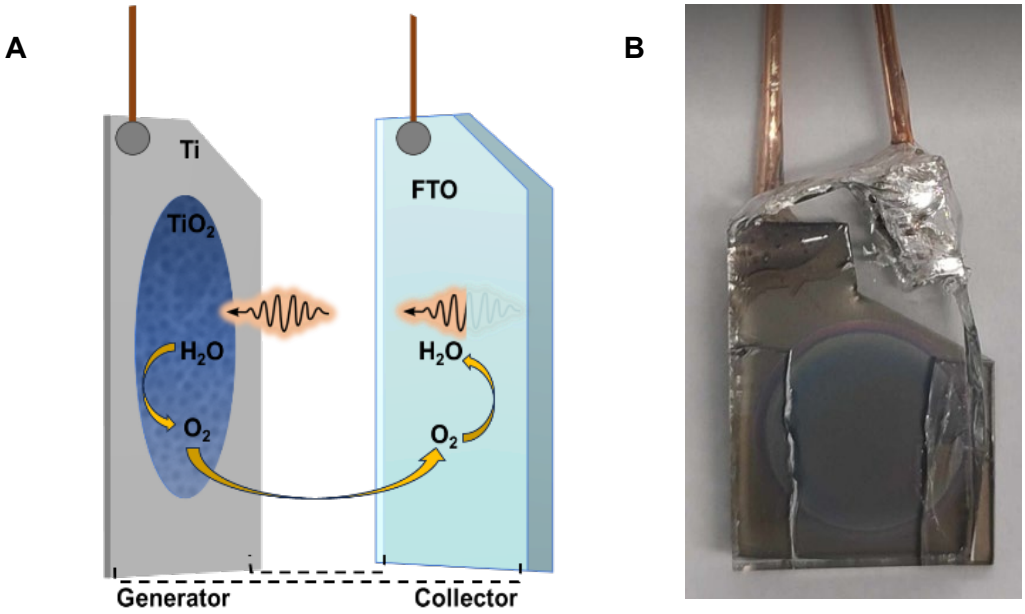

Figure S2. (A) Schematic and (B) picture of collector-generator assembly.

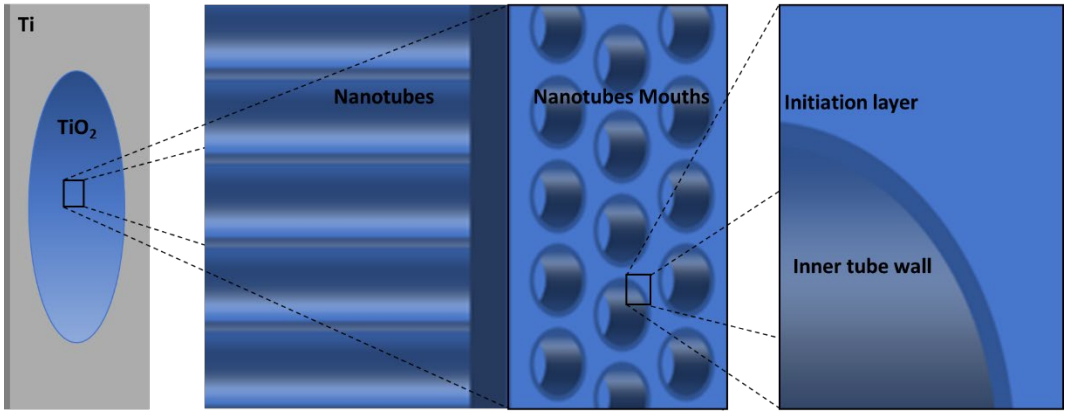

Scheme S2. Expected morphology of the TiO_2 NTs photoelectrode. The working surface for functionalization is the nanotube mouths composed of the initiation layer and inner tube wall.

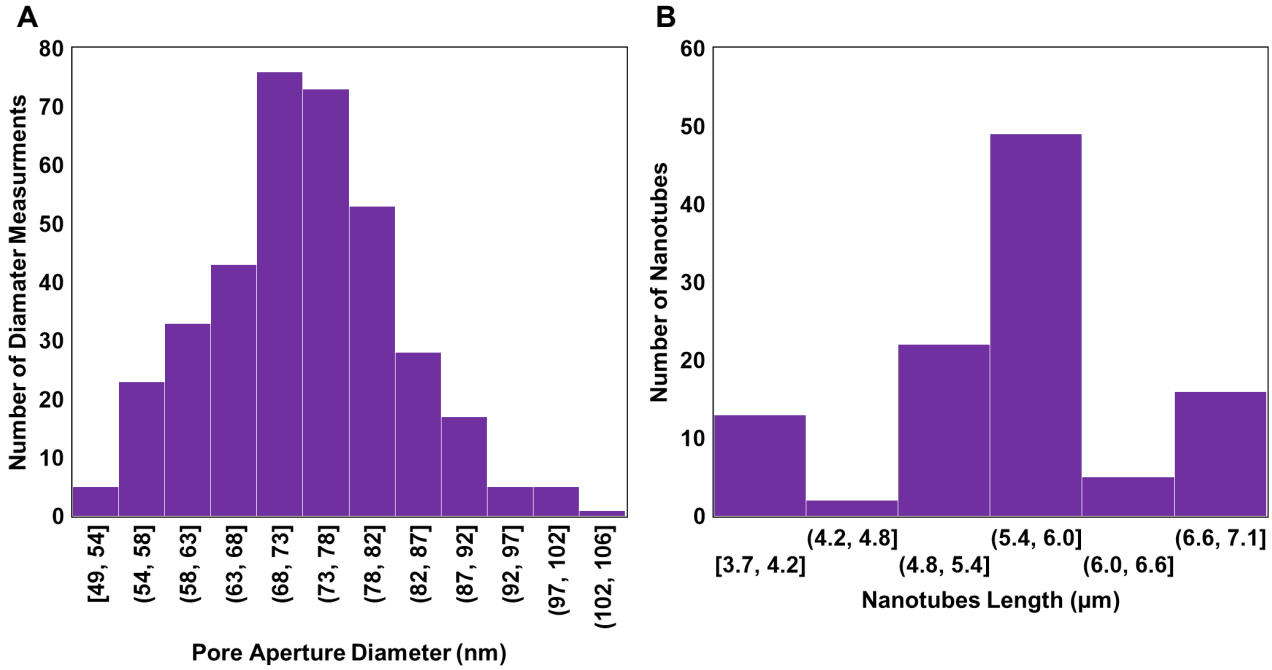

Figure S3. (A) Pore aperture diameter distribution from 2 measurements per pore for 181 nanotubes and (B) Nanotube length distribution measured from 107 nanotubes across 4 array fragments using ImageJ.

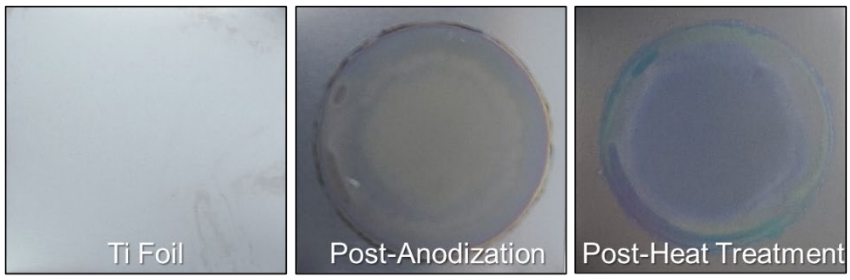

Figure S4. Pictures of TiO_2 NTs photoelectrode from resulting anodization and annealing.

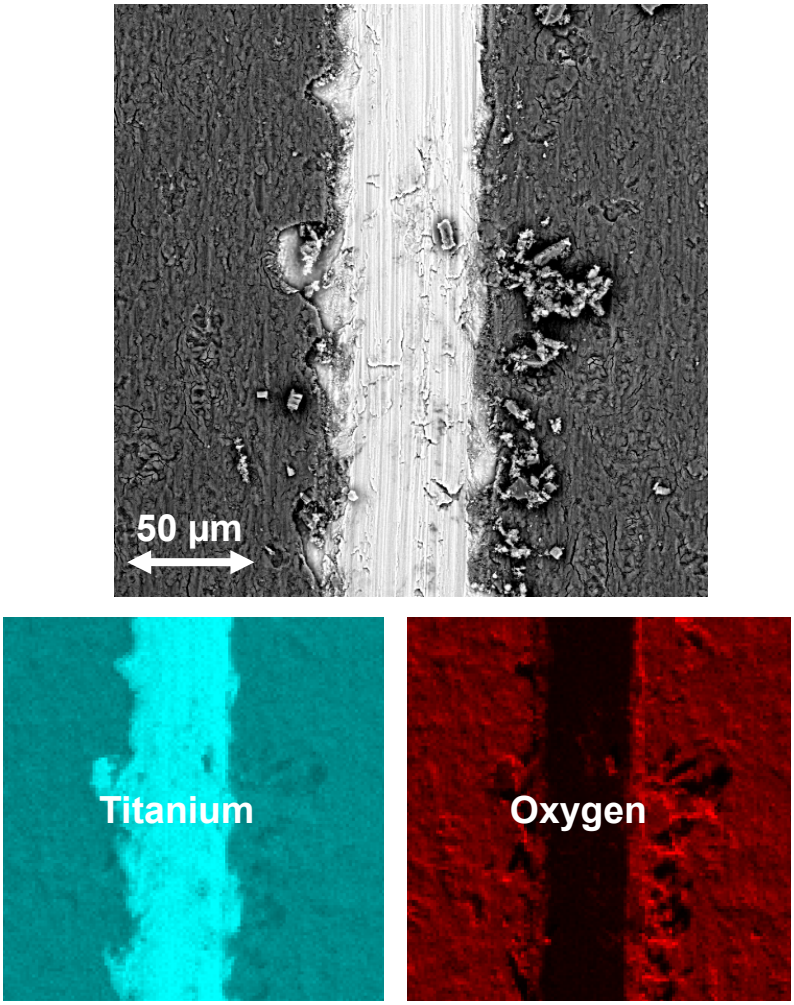

Figure S5. SEM micrograph of TiO_2 NTs and elemental maps of titanium and oxygen.

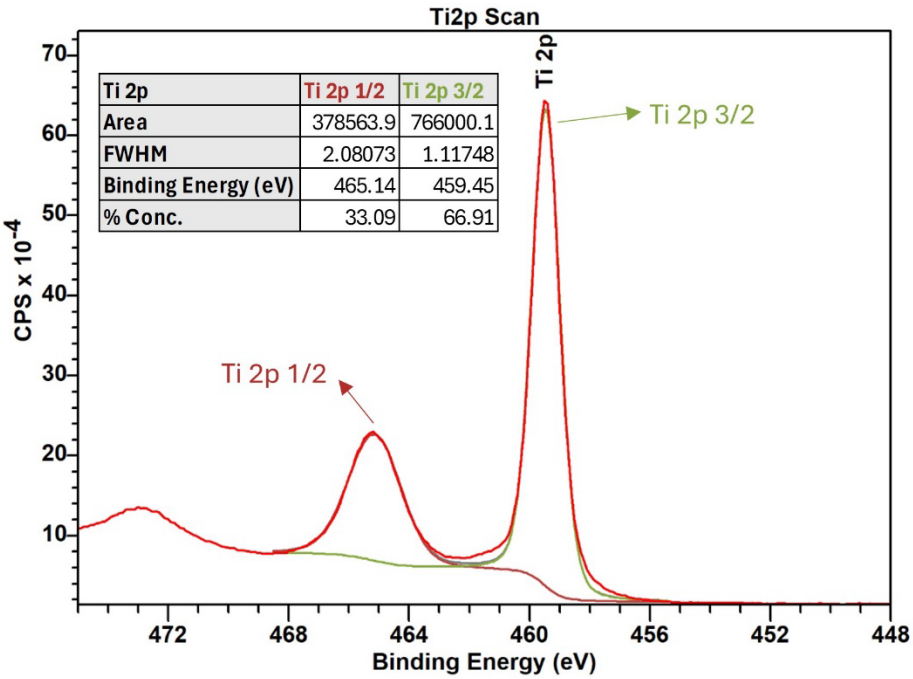

Ti 2p	Ti 2p 1/2	Ti 2p 3/2
Area	378563.9	766000.1
FWHM	2.08073	1.11748
Binding Energy (eV)	465.14	459.45
% Conc.	33.09	66.91

Figure S6. XPS high resolution scan of TiO_2 NTs in the titanium binding energy region.

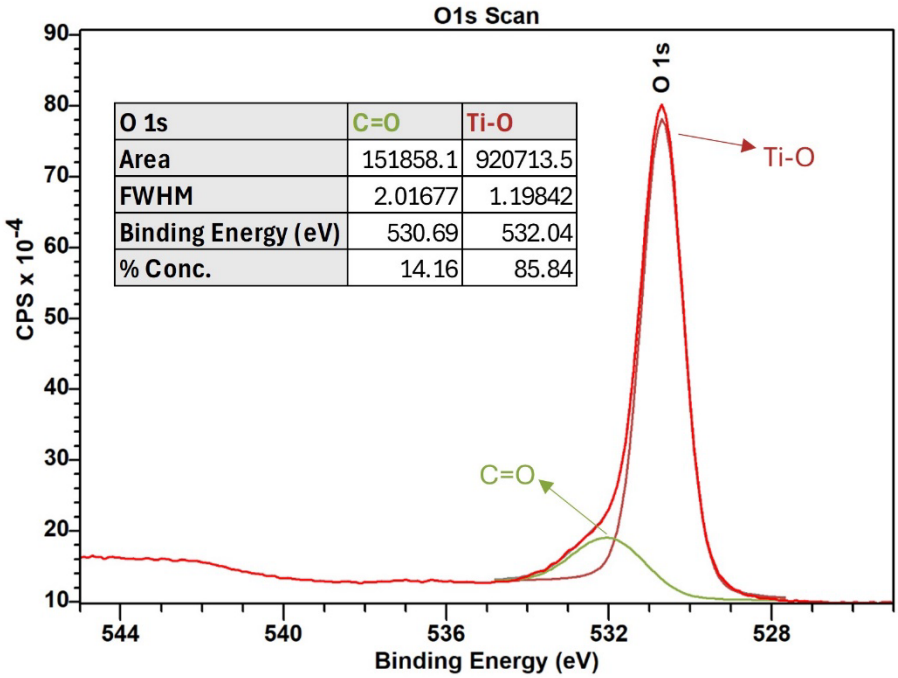

O 1s	C=O	Ti-O
Area	151858.1	920713.5
FWHM	2.01677	1.19842
Binding Energy (eV)	530.69	532.04
% Conc.	14.16	85.84

Figure S7. XPS high resolution scan of TiO_2 NTs in the oxygen binding energy region.

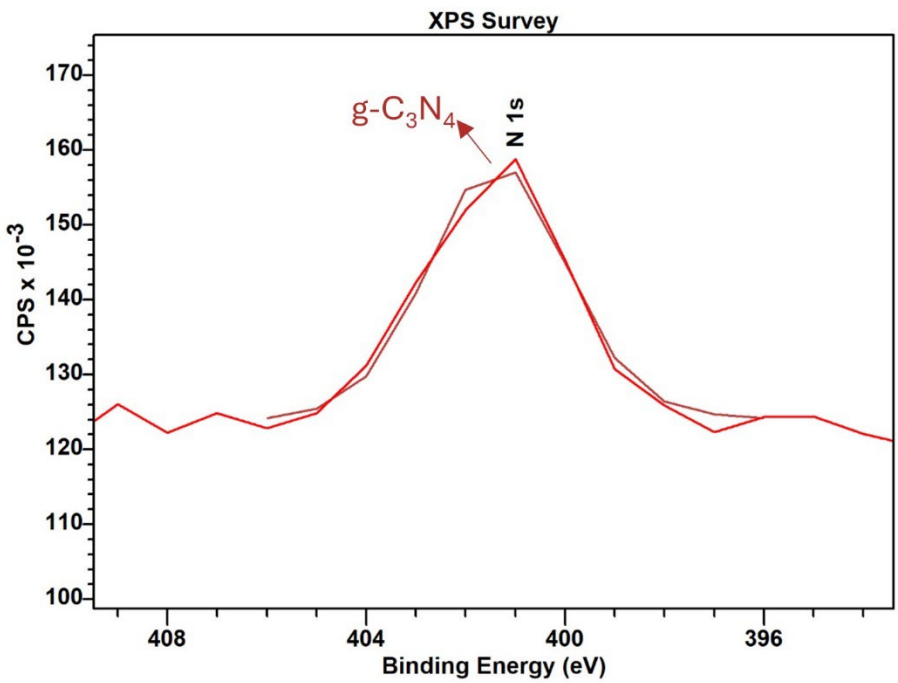

Figure S8. XPS binding energy of nitrogen in TiO_2 NTs.

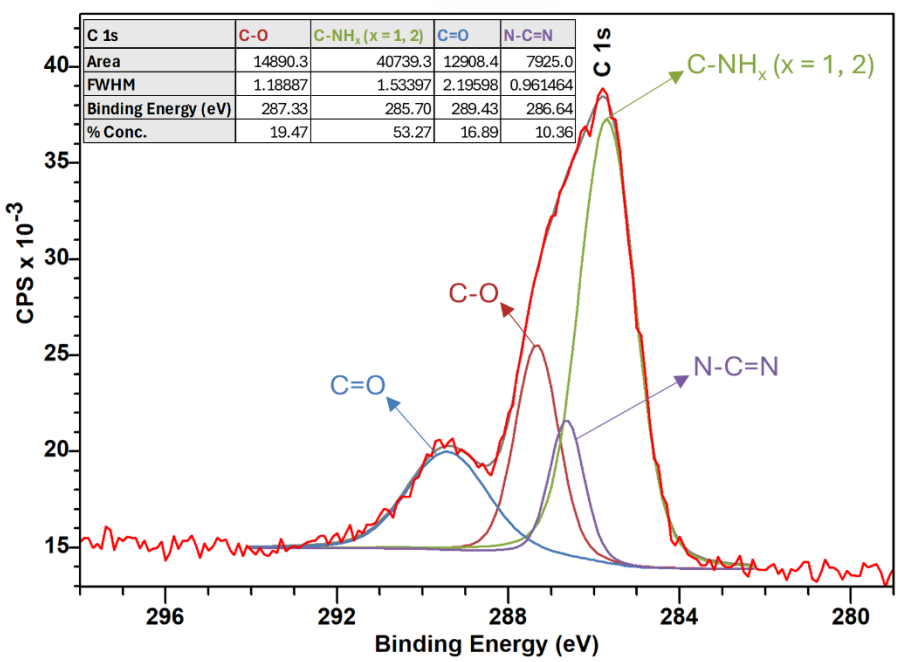

C 1s	C-O	C-NHx (x = 1, 2)	C=O	N-C=N
Area	14890.3	40739.3	12908.4	7925.0
FWHM	1.18887	1.53397	2.19598	0.961464
Binding Energy (eV)	287.33	285.70	289.43	286.64
% Conc.	19.47	53.27	16.89	10.36

Figure S9. XPS high resolution scan of TiO_2 NTs in the carbon binding energy region.

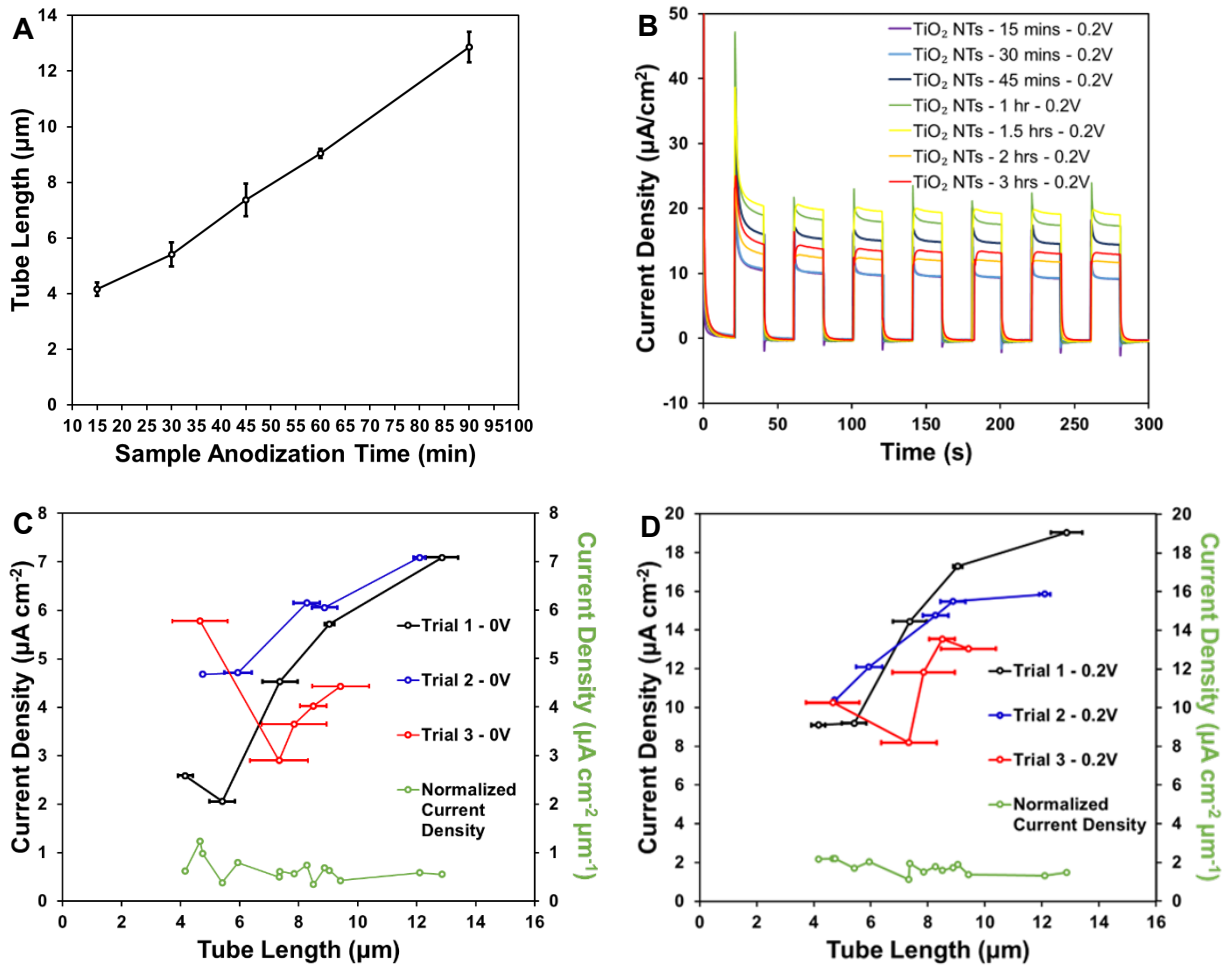

Figure S10. Photocurrent normalization to nanotube length. (A) Tube length measured by cross-sectional SEM depending on anodization period, (B) Chopped-light chronoamperometry of TiO_2 NTs samples grown for periods of 15, 30, 45, 60, 90, 120, and 180 minutes. (C) and (D) Current density normalization at 0 V and 0.2 V over tube length associated to the sample. All experiments were conducted in aqueous 0.1 M Na_2SO_4 solution with the photoelectrode as working electrode, platinum mesh as counter electrode and a saturated calomel electrode as reference electrode.

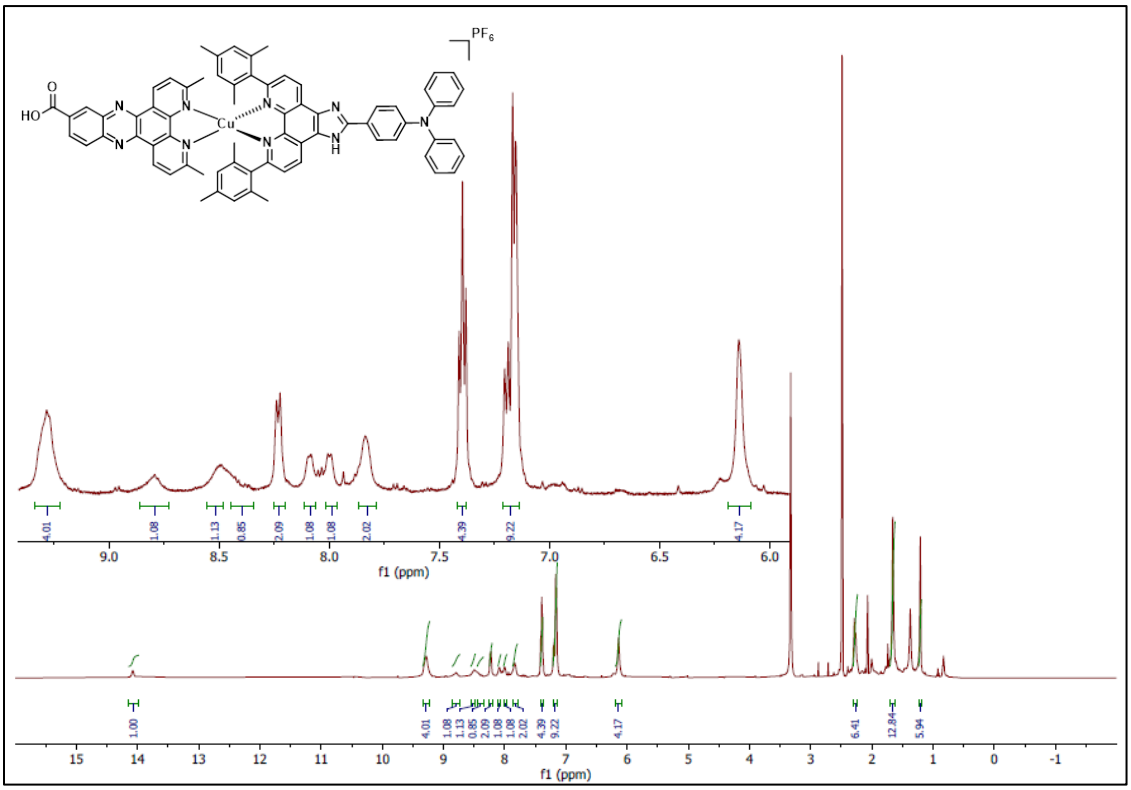

Figure S11. ^{1}H NMR spectrum of **A-Cu(I)-D** in DMSO-d_6 recorded on a 500 MHz Varian spectrometer.

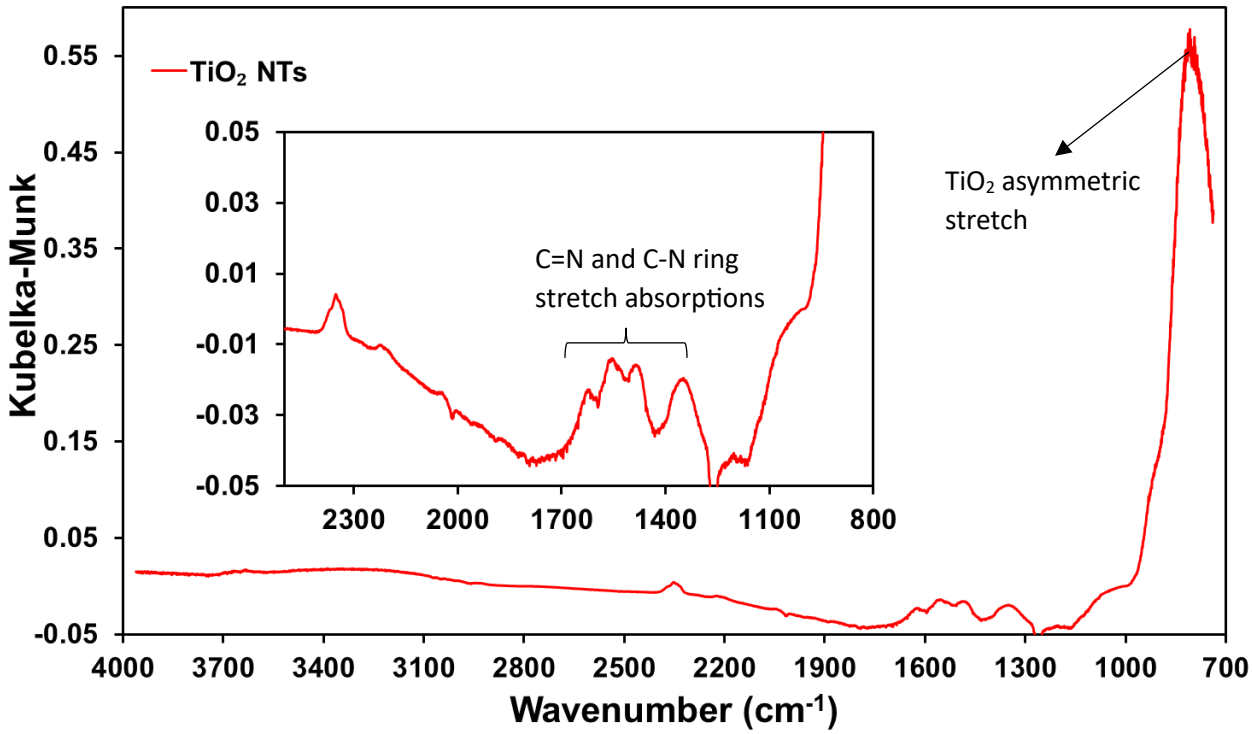

Figure S12. DRIFTS analysis of TiO_2 NTs baselined against Ti foil.

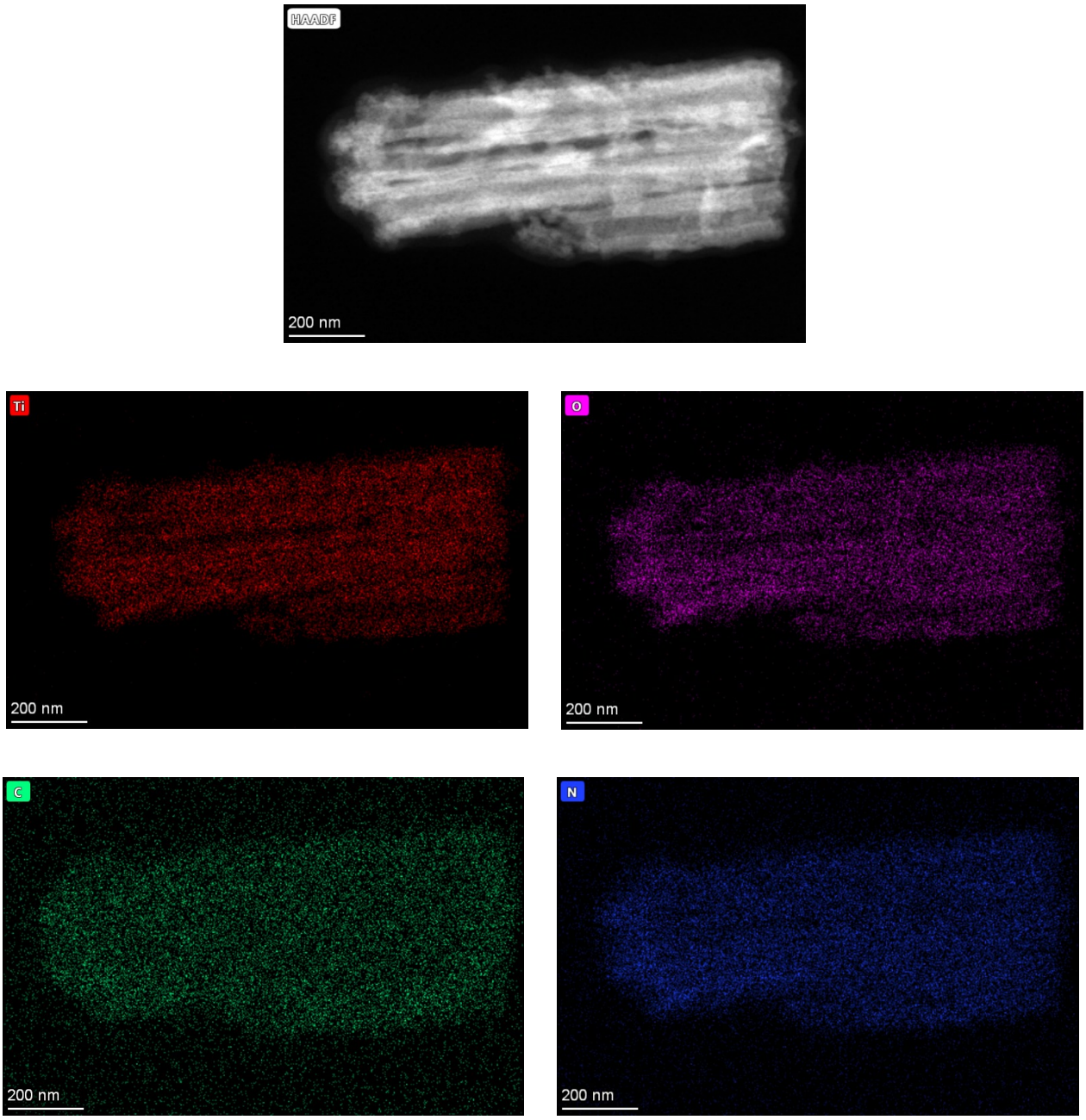

Figure S13. HAADF and elemental mapping of TiO_2 NTs.

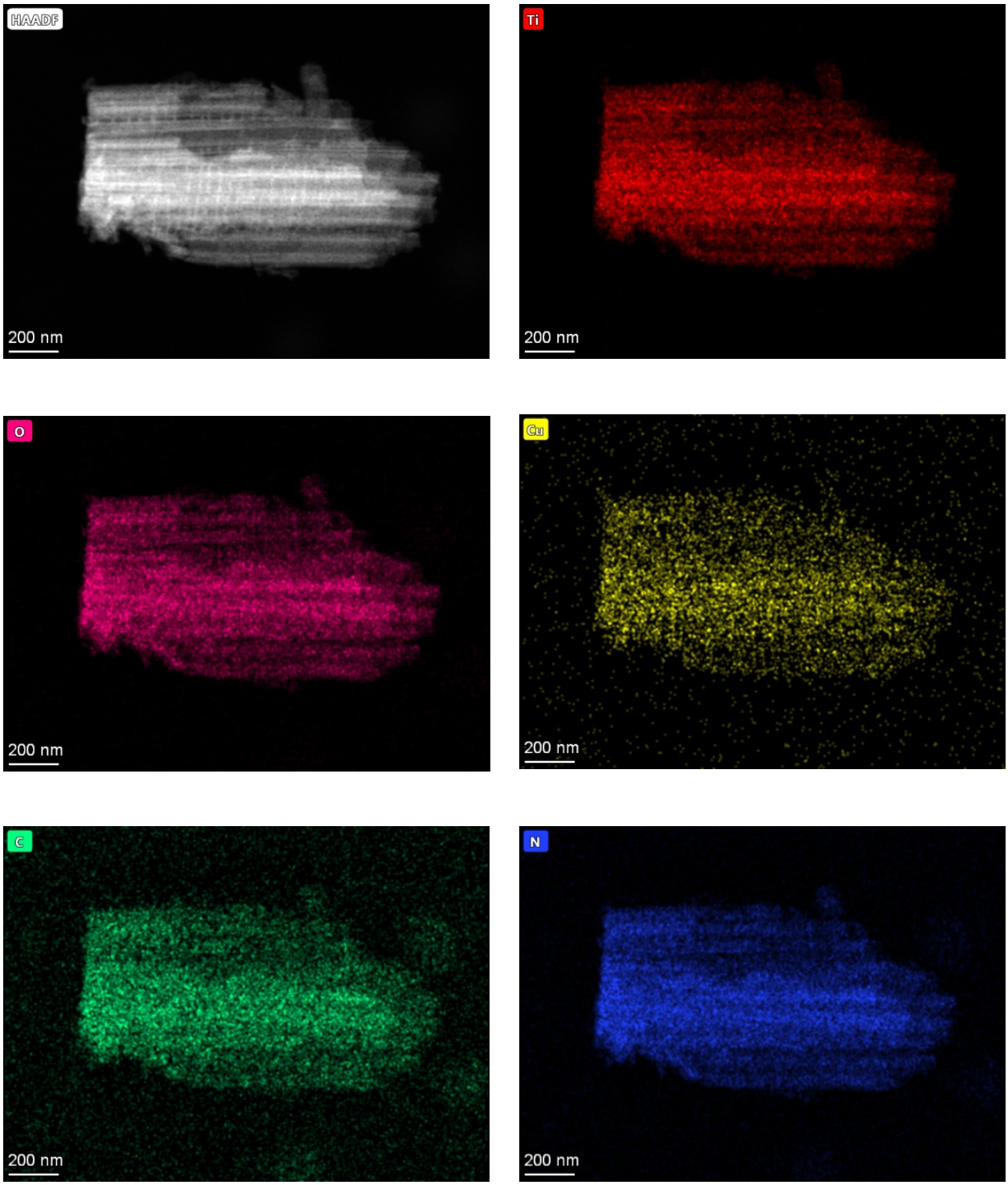

Figure S14. HAADF and elemental mapping of TiO_2 NTs|A-Cu(I)-D.

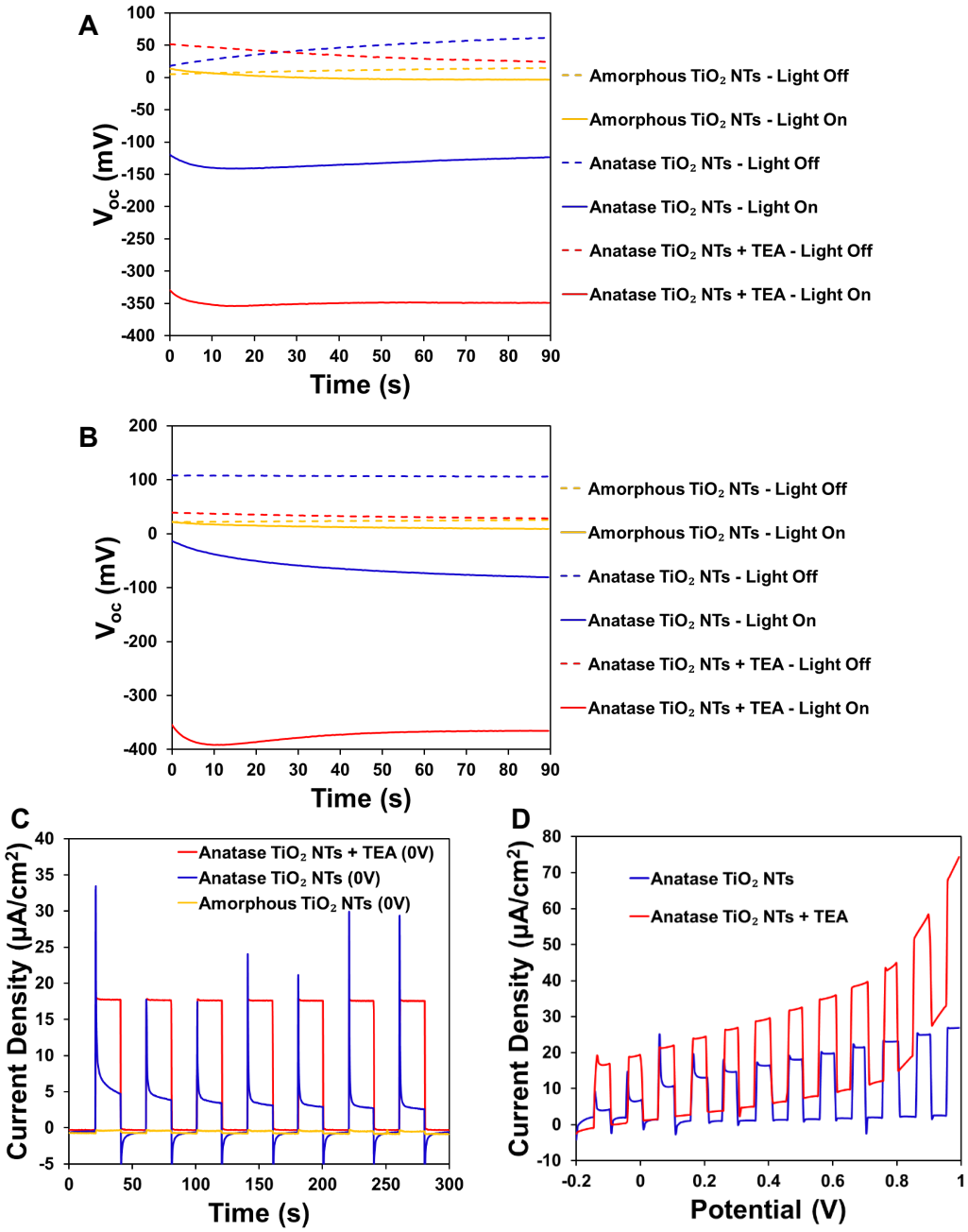

Figure S15. OCP measurement (A) before and (B) after photoelectrochemical testing. (C) Chopped-light chronoamperometry experiments of amorphous TiO_2 NTs (yellow), anatase TiO_2 NTs (blue) and anatase TiO_2 NTs with triethylamine as a sacrificial electron donor (red) at 0 V vs SCE. (D) Chopped-light linear sweep voltammetry with and without addition of sacrificial electron donor TEA. Photoelectrochemical testing conducted in aqueous 0.1 M Na_2SO_4 pH 8.9 solution with the photoelectrode as a working electrode, platinum mesh as a counter electrode and a saturated calomel electrode as a reference electrode.

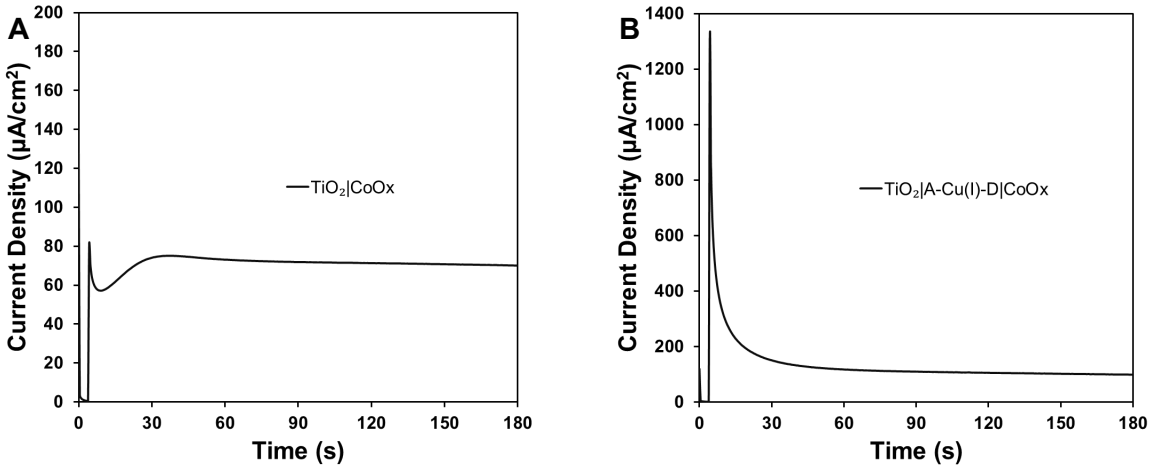

Figure S16. Chronoamperogram of CoOx photoelectrochemical deposition on (A) TiO_2 NTs photoelectrode and (B) TiO_2 NTs|A-Cu(I)-D photoelectrode. Conditions: Aqueous 0.5 mM $Co(NO_3)_2$ in 0.1 M pH 7 phosphate buffer (KPi) held at +0.2 V versus SCE under a white light emitting diode for 180 seconds. WE: 2 mm Pt button; RE: Ag wire; CE: Pt mesh. in

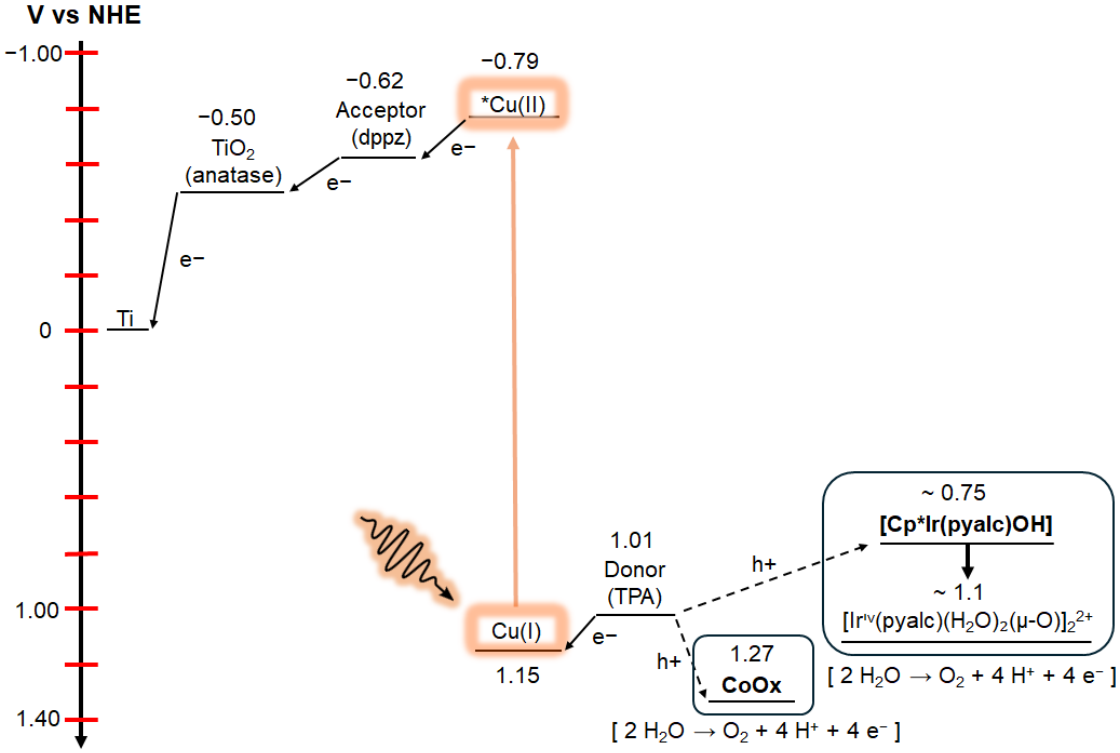

Scheme S3. Proposed energy level diagram for TiO_2 NTs|A-Cu(I)-D with the presence of WOCs using electrochemical potentials of all redox components. Anatase TiO_2 conduction band position is taken from Li *et al.*,[1] **A-Cu(I)-D** excited state and redox species are from our previous work,[2] CoOx regeneration position is taken from Jewell *et al.*,[3] and [Cp*Ir(pyalc)OH] precursor transformation and water oxidation catalysis was taken from Sheehan *et al.*[4] All potentials are reported at pH 7.

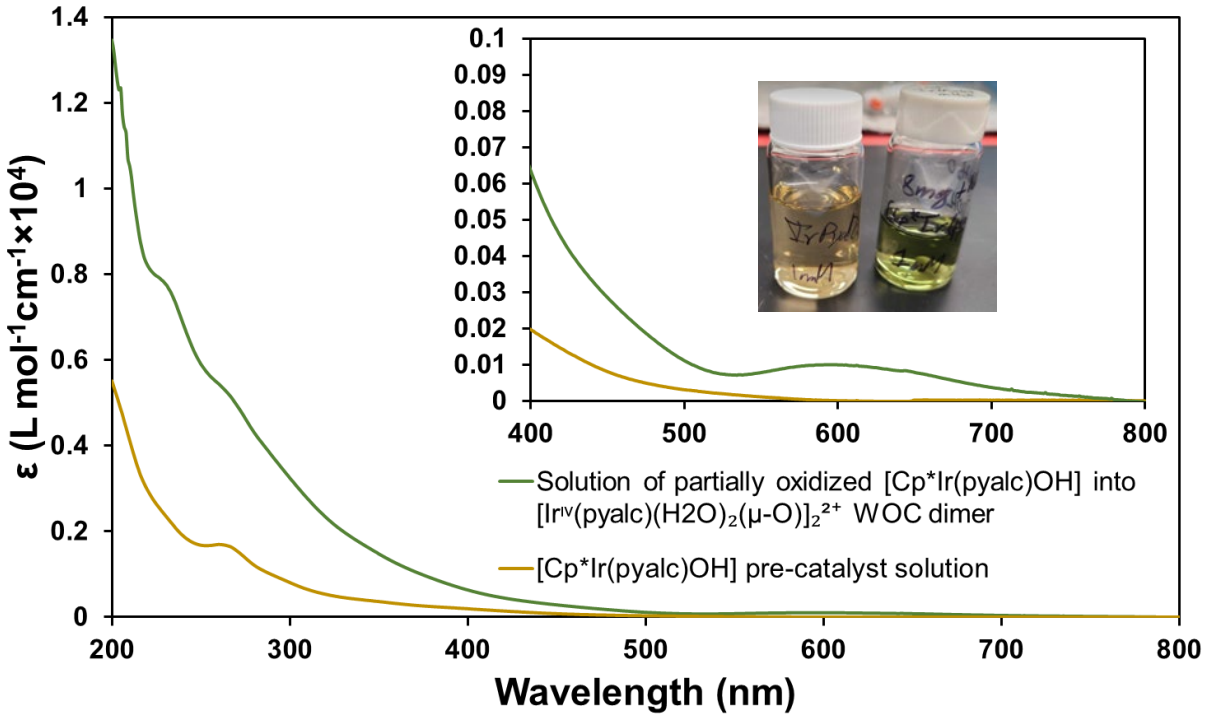

Figure S17. UV-Vis of [Cp*Ir(pyalc)OH] in aqueous 0.1 M Na_2SO_4 pH 8.9 solution used for photoelectrochemistry.

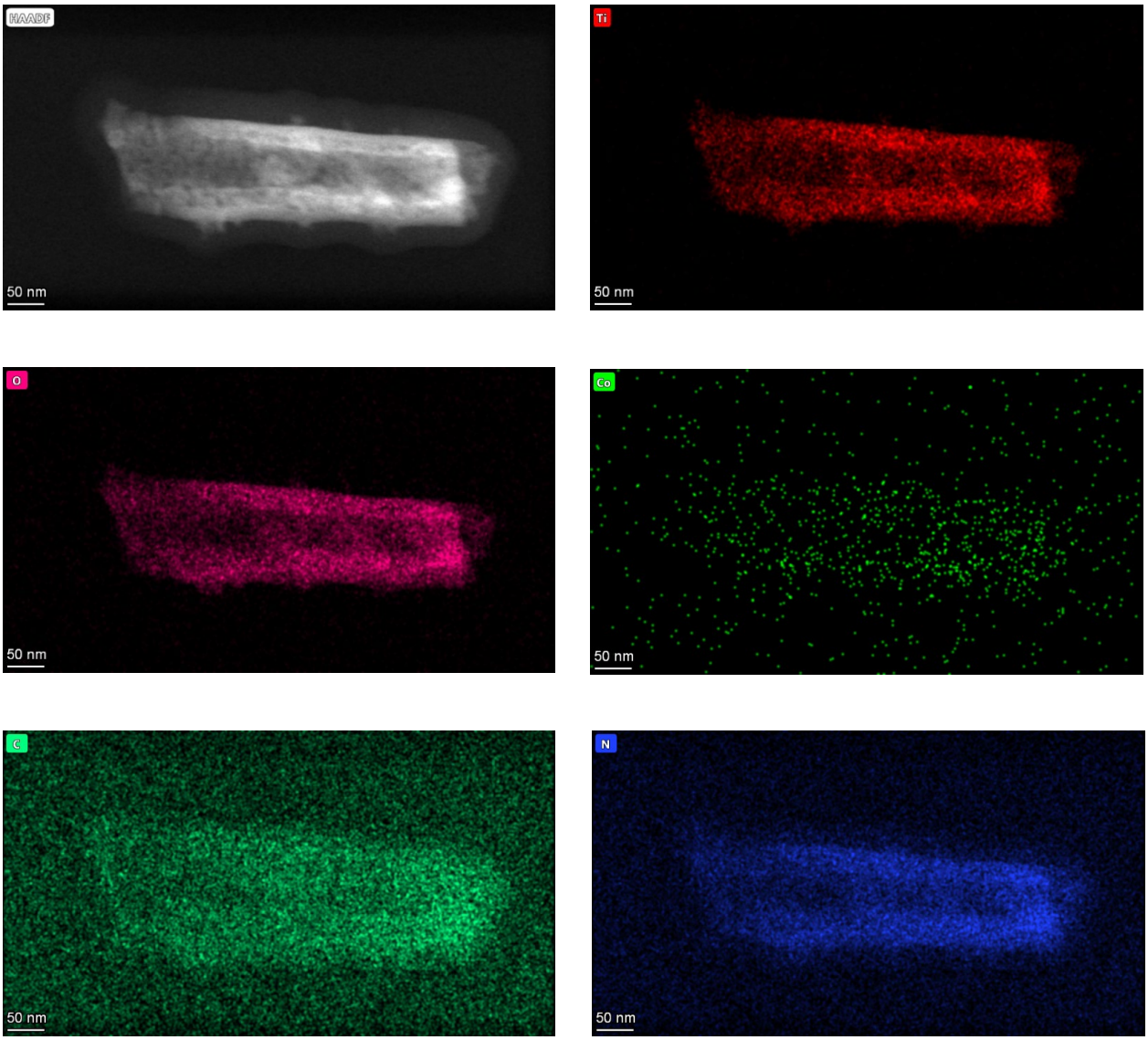

Figure S18. HAADF and elemental mapping of TiO_2 NTs|CoOx.

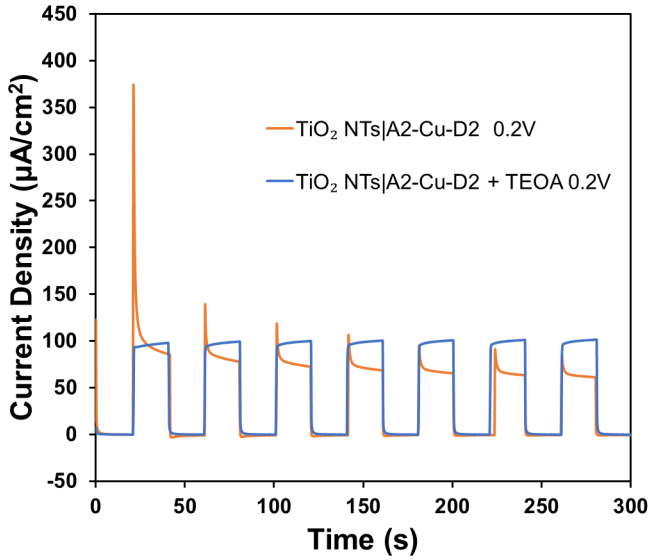

Figure S19. Chopped-light chronoamperogram of TiO_2 NTs|A-Cu(I)-D with the addition of sacrificial electron donor TEOA. Photoelectrochemical testing conducted in aqueous 0.1 M Na_2SO_4 pH 8.9 solution with the photoelectrode as a working electrode, platinum mesh as a counter electrode and a saturated calomel electrode as a reference electrode.

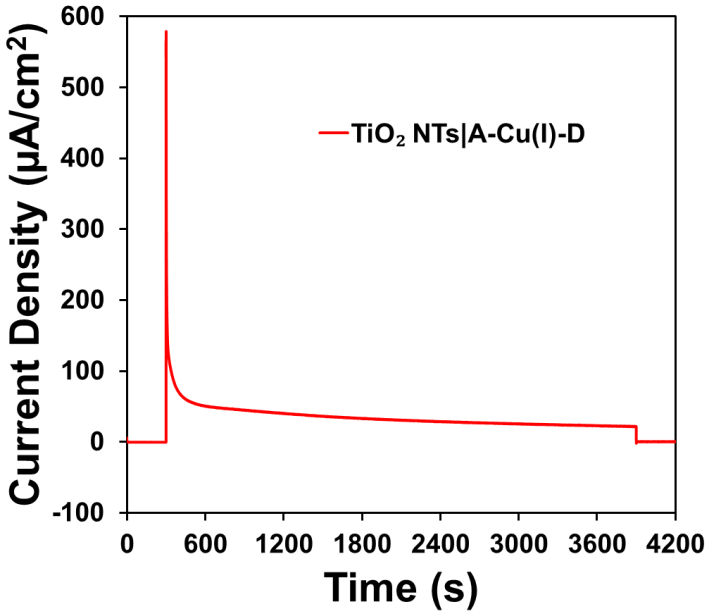

Figure S20. Chronoamperometry experiment of TiO_2 NTs|A-Cu(I)-D illuminated with a 540 mW/cm^2 single white LED over the period of 1 hour. Photoelectrochemical testing conducted in aqueous 0.1 M Na_2SO_4 pH 8.9 solution with the photoelectrode as a working electrode, platinum mesh as a counter electrode and a saturated calomel electrode as a reference electrode.

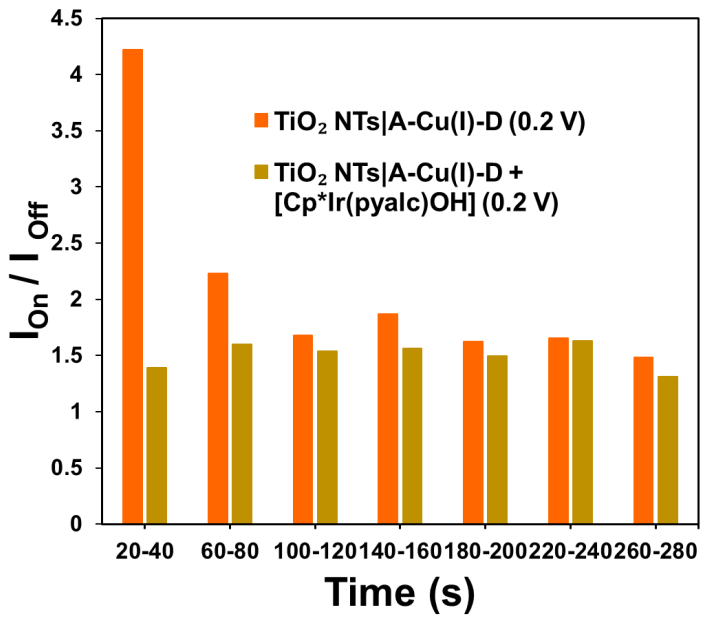

Figure S21. Photocurrent ratios of photocurrent at the beginning of light on versus at the end of light on in the absence (Orange) and presence (Yellow) of [Cp*Ir(pyalc)OH].

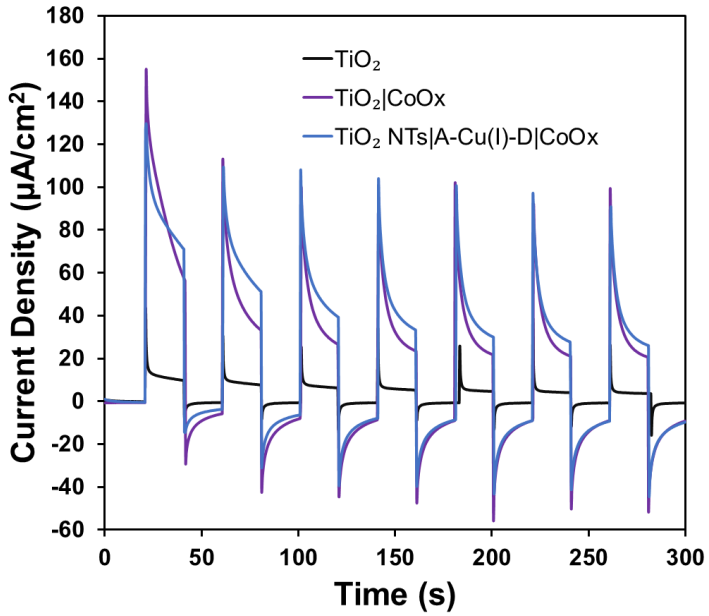

Figure S22. Chopped-light chronoamperogram at 0 V vs SCE of photoanodes with CoOx photoelectrochemically deposited. Photoelectrochemical testing conducted in aqueous 0.1 M Na_2SO_4 pH 8.9 solution with the photoelectrode as a working electrode, platinum mesh as a counter electrode and a saturated calomel electrode as a reference electrode.

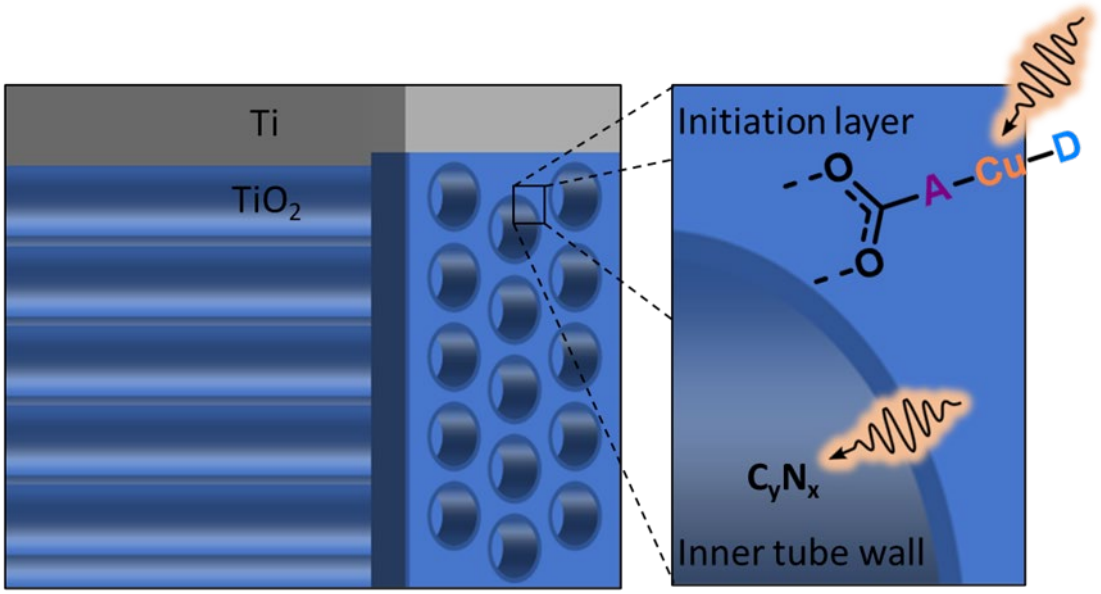

Scheme S4. Photoaction scheme. Photocurrent originating from **A-Cu(I)-D** decorated on the initiation layer using low power density light source and photocurrent generated using high power density light source originating from graphitic carbon and/or graphitic nitrides incorporated in the inner tube wall.

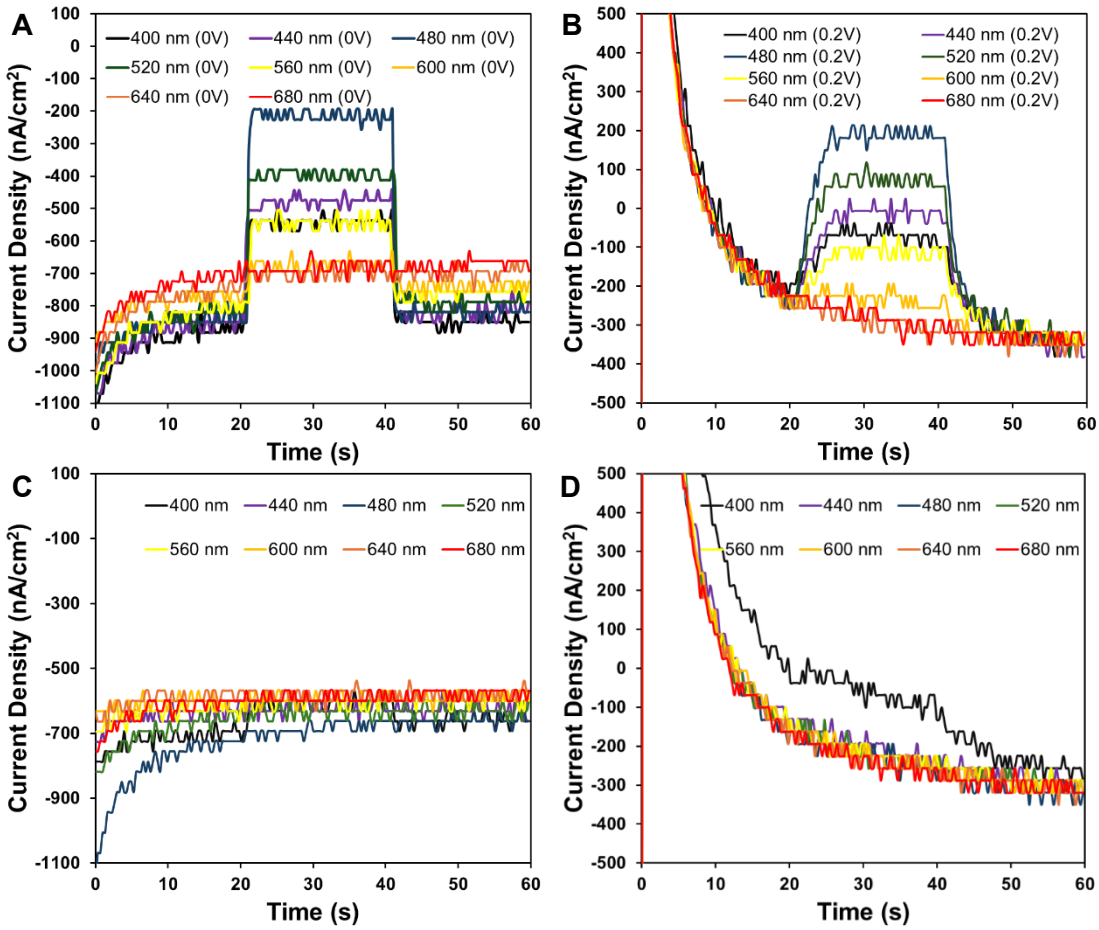

Figure S23. TiO_2 NTs|A-Cu(I)-D with an applied potential of (A) 0 V and (B) 0.2 V vs SCE illuminated with an Oriel Corp 77503 Fiber Optic Illuminator as light source with < 1 mW/cm^2 power density. TiO_2 NTs with an applied potential of (C) 0 V and (D) 0.2 V vs SCE was used as control. WE: Photoanode; Ref.: Saturated calomel electrode; CE: Pt mesh; Electrolyte solution: aqueous 0.1 M Na_2SO_4 pH 8.9.

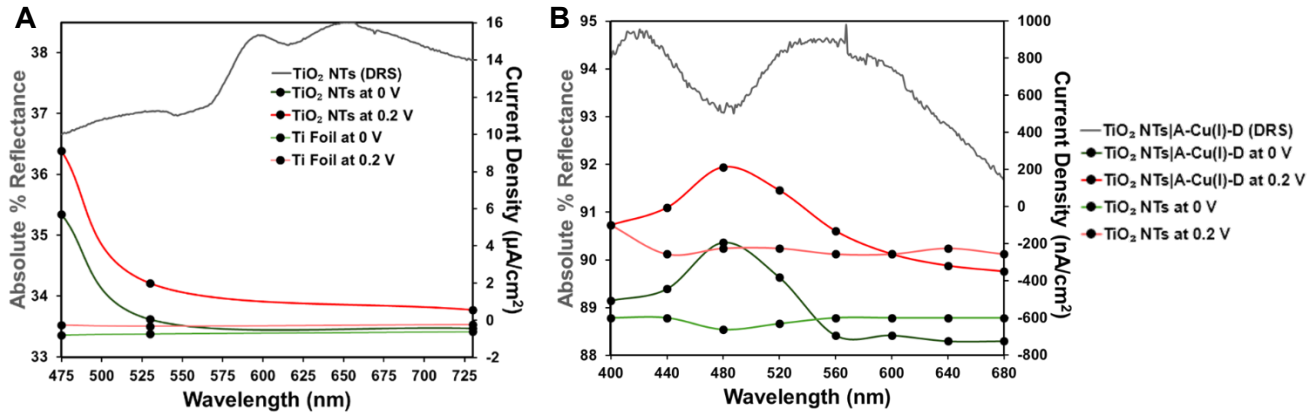

Figure S24. Photoaction spectra of (A) TiO_2 NTs and (B) TiO_2 NTs|A-Cu(I)-D.

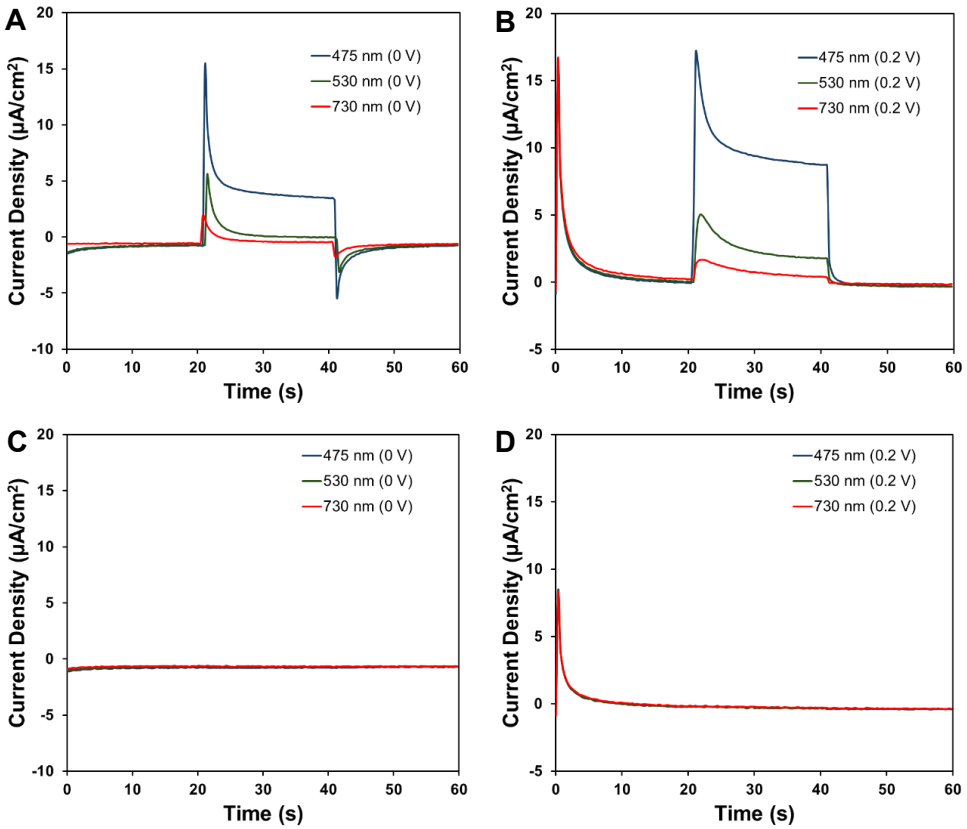

Figure S25. Single LEDs Chopped-light chronoamperometry experiment on TiO_2 NTs with an applied potential of (A) 0 V and (B) 0.2 V vs SCE illuminated with a 65 mW/cm^2 single blue LED (475 nm), a 92 mW/cm^2 single green LED (530 nm) and a 104 mW/cm^2 single red LED (730 nm). Ti Foil with an applied potential of (C) 0 V and (D) 0.2 V vs SCE was used as control. WE: Photoanode; Ref.: Saturated calomel electrode; CE: Pt mesh; Electrolyte solution: aqueous 0.1 M Na_2SO_4 pH 8.9.

Wavelength (nm)	IPCE % of TiO_2 NTs at 0 V	IPCE % of TiO_2 NTs at 0.2 V
475	2.29	3.66
530	0.02	0.51
730	0.00	0.09

Table S1. IPCE% of TiO_2 NTs

Wavelength (nm)	IPCE % of TiO_2 NTs|A-Cu(I)-D at 0 V	IPCE % of TiO_2 NTs|A-Cu(I)-D at 0.2 V
480	1.02	1.21
520	0.76	0.88
560	0.16	0.44
600	0.05	0.20
640	0.00	0.09
680	0.00	0.04

Table S2. IPCE% of TiO_2 NTs|A-Cu(I)-D

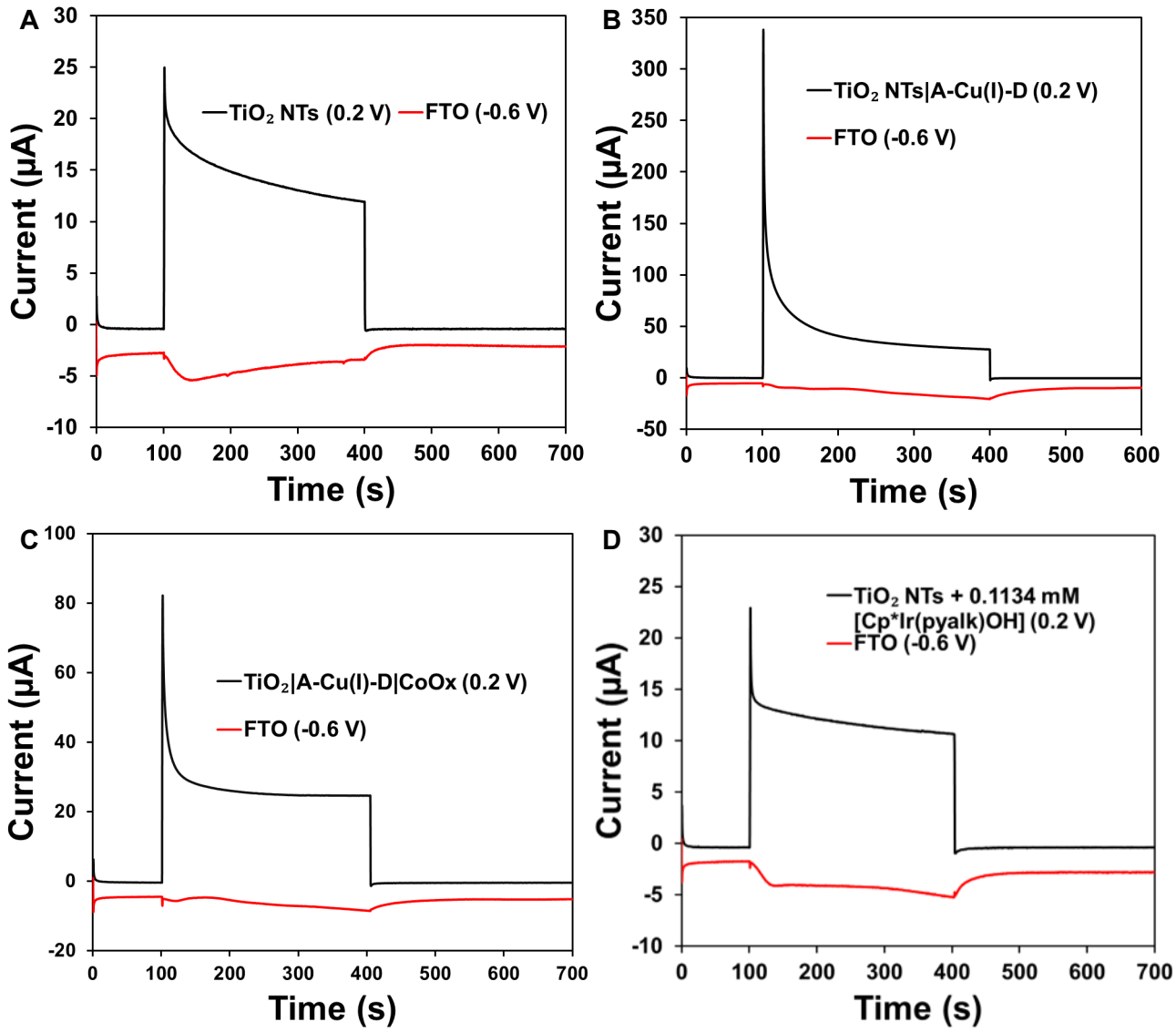

Figure S26. Collector-generator dual working electrode experiment on (A) TiO_2 NTs, (B) TiO_2 NTs|A-Cu(I)-D, (C) TiO_2 NTs|A-Cu(I)-D|CoOx and (D) TiO_2 NTs + 0.1134 mM [Cp*Ir(pyalc)OH] in aqueous 0.1 M Na_2SO_4 pH 8.9. The generator electrode was held at 0.2 V and illuminated with white light. The collector electrode was held at -0.6 V. Reference electrode: saturated calomel electrode. Counter electrode: platinum mesh.

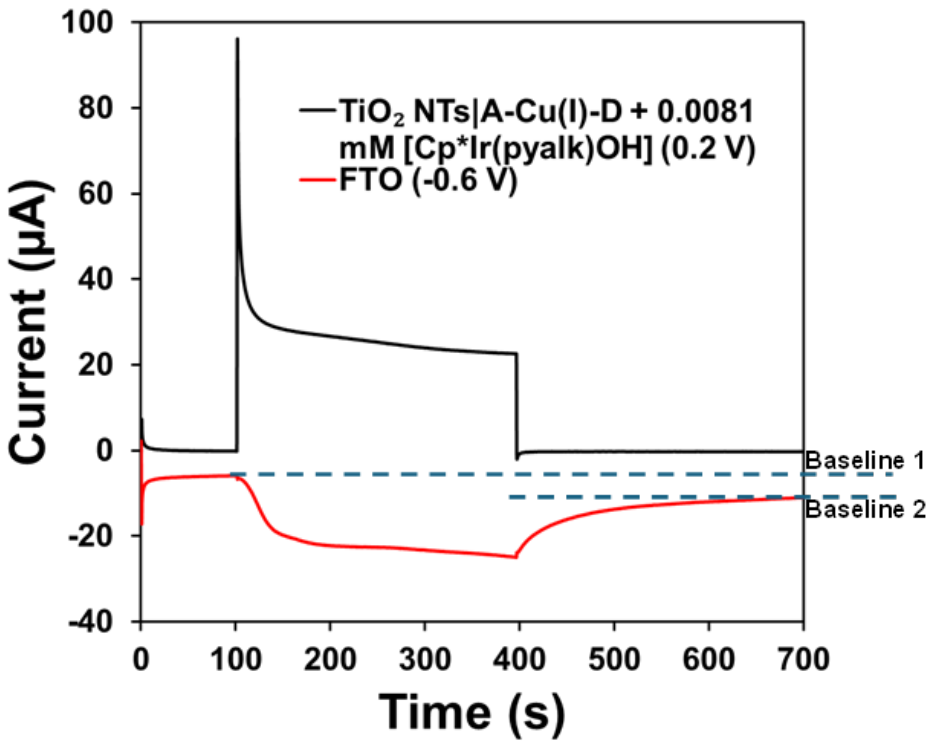

Photoanode (MOx|PS|WOC or + WOC)	Faradaic Efficiency (%) 100-400s (Baseline 1)	Faradaic Efficiency (%) 100-400s (Baseline 1) + 400-700s (Baseline 2)
TiO_2 NTs|A-Cu(I)-D|CoOx	11	13
TiO_2 NTs	15	15
TiO_2 NTs + 0.1134 mM [Cp*Ir(pyalc)OH]	29	44
TiO_2 NTs|A-Cu(I)-D	27	32
TiO_2 NTs|A-Cu(I)-D + 0.0081 mM [Cp*Ir(pyalc)OH]	84	99
TiO_2 NTs|A-Cu(I)-D + 0.1134 mM [Cp*Ir(pyalc)OH]	64	82

Q_{gen} and Q_{col} are given by integrating the area between the respective current generated and the baseline.

Example given for TiO_2 NTs|A-Cu(I)-D + 0.0081 mM [Cp*Ir(pyalc)OH]:

$$\boldsymbol{Q_{gen} = 7814\ \mu C}$$

$$\boldsymbol{Q_{col} = 4572\ \mu C}$$

$$\boldsymbol{\eta_{coleff} = 70\% = 0.7}$$

$$\boldsymbol{\eta_{O_2} = \left(\frac{Q_{col}}{Q_{gen}}\right)\left(\frac{1}{\eta_{coleff}}\right) = \left(\frac{4572\ \cancel{\mu C}}{7814\ \cancel{\mu C}}\right)\left(\frac{1}{0.7}\right) = 0.8359 = 84\%}$$

Figure S27. Faradaic efficiency calculation.

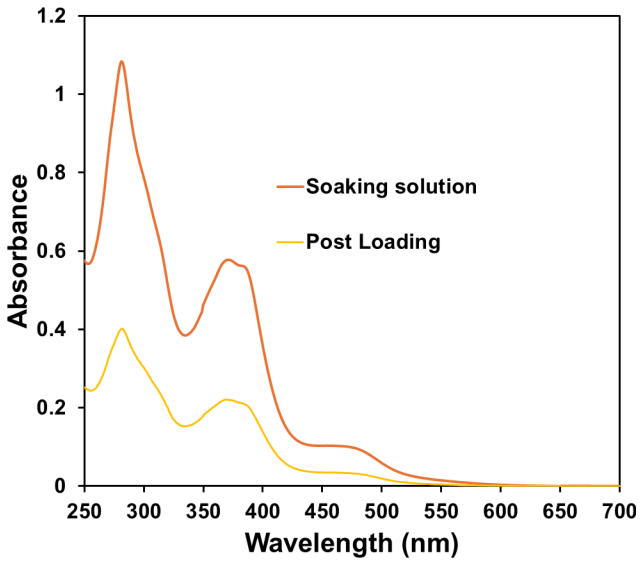

Loading calculations:

Molar absorptivity constant (ε) for MLCT transition in A-Cu(I)-D = 7900 L mol^{-1} cm^{-1}

Beer Lambert Law: A = ε C l = (ε m l) / V

Concentration of A-Cu(I)-D: C = A / ε l

Optical pathlength of the cuvette (l) = 1 cm

Fresh soaking solution = 0.0121 mM

Post-loading soaking solution = 0.0040 mM

Concentration loaded on TiO_2 NTs =

0.0121 mM – 0.0040 mM = 0.0081 mM

Loading on TiO_2 NTs =

$$\frac{8.1 \times 10^{-6}\, M \times 0.004\, L}{1\, cm^2} = 3.24 \times 10^{-8}\, mol/cm^2$$

Figure S28. **A-Cu(I)-D** loading calculation on TiO_2 NTs.

References

1. Li, F.; Fan, K.; Xu, B.; Gabrielsson, E.; Daniel, Q.; Li, L.; Sun, L., *J. Am. Chem. Soc.*, **2015**, *137*, 9153–9159.
2. Z. Singh, S. Kamal and M. B. Majewski, *J. Phys. Chem. C*, **2022**, *126*, 16732–16743.
3. C. F. Jewell, A. Subramanian, C.-Y. Nam and R. G. Finke, *ACS Appl. Mater. Interfaces*, **2022**, *14*, 25326–25336.
4. S. W. Sheehan, J. M. Thomsen, U. Hintermair, R. H. Crabtree, G. W. Brudvig and C. A. Schmuttenmaer, *Nat. Commun.*, **2015**, *6*, 6469.